Supporting Information

Highly sensitive and reusable electrochemical mercury biosensor based on tunable vertical single-walled carbon nanotubes and a target recycling strategy

Lei Shi,[a] Yan Wang,[a] Zhenyu Chu,[b] Yu Yin,[c] Danfeng Jiang,[b] Jingyi Luo,[b] Shiming Ding*[a] and Wanqin Jin*[b]

[a]State Key Laboratory of Lake Science and Environment, Nanjing Institute of Geography and Limnology, Chinese Academy of Sciences, Nanjing 210008, P. R. China.

[b]State Key Laboratory of Materials-Oriented Chemical Engineering, College of Chemical Engineering, Nanjing Tech University, Nanjing 210009, P. R. China.

[c]School of Environmental and Chemical Engineering, Jiangsu University of Science and Technology, Zhenjiang 212003, P. R. China.

The binding energies (BEs) at around 84, 164, 285 and 399 eV are attributed to Au4f, S2p, C1s and N1s species respectively (Fig. S1A). The BE in N1s spectrum at about 399.4 eV is ascribed to the terminal amine group of 4-aminothiophenol (Fig. S1B).

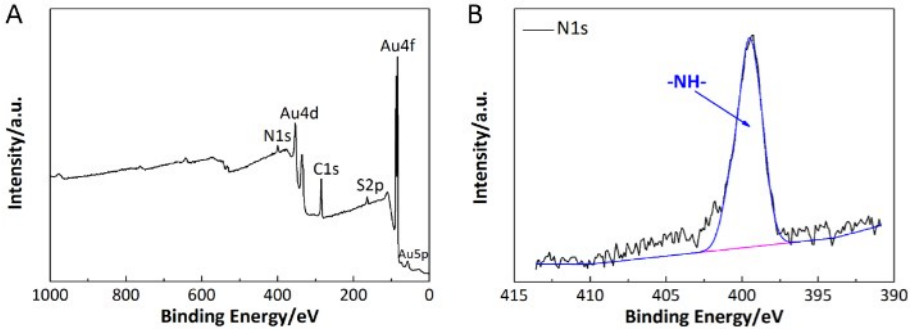

Fig. S1 (A) XPS survey, and (B) N1s spectra of R-SAM/Au.

DFT simulations were introduced to investigate conformations of SAMs based on the repeated slab approach for periodic surface and interface systems, in which SAMs/Au(001) interface systems composed of a slab of Au(001) and a monolayer of 2-aminoethanethiol or 4-aminothiophenol molecules were constructed. The geometry optimizations were performed with the Cambridge Sequential Total Energy Package (CASTEP) module of Materials Studio (Accelrys Software Inc.). To give a clear observation on SAMs/Au(001) interfaces, simulation models were simplified here and only the top layer of Au atoms interacted with SAMs was displayed.

In order to show the stability of different conformations of SAMs, we calculated the total energy of R-SAM/Au(001) and S-SAM/Au(001) respectively. The total enery in Fig. S2A and Fig. S2B were -25670.9796 eV and -25683.7191 eV respectively. Meanwhile, the total enery in Fig. S2D and Fig. S2E were -27521.3188 eV and -27544.2049 eV respectively. It is found that the SAMs with lower total energy were obtained after the geometry optimizations, indicating that more stable conformations were acquired.

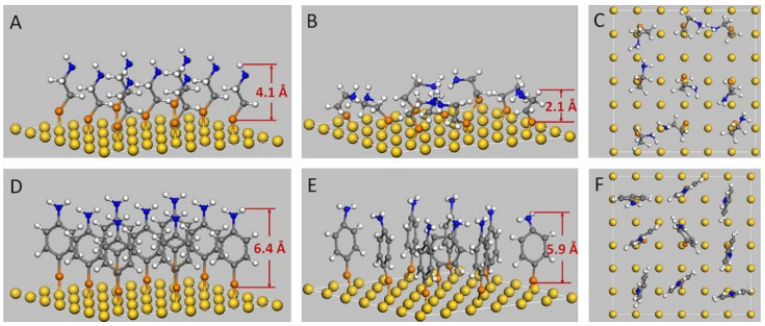

Fig. S2 DFT simulations of S-SAM and R-SAM adsorbed on Au(001) surfaces. Cross views of S-SAM, (A) before and (B) after the conformational optimizations, (C) Top view of S-SAM. Cross views of R-SAM, (D) before and (E) after the conformational optimizations, (F) Top view of R-SAM.

The BEs at 84, 164, 285, 399 and 530 eV are attributed to Au4f, S2p, C1s, N1s and O1s species respectively (Fig. S3A). The BE in N1s spectrum at 400.2 eV is attributed to the NH–C=O, confirming the chemical immobilization of SWCNTs on the R-SAM/Au, and the BE at 399.4 eV is ascribed to the uncombined amine group of 4-aminothiophenol (inset in Fig. S3A). Besides, the BEs in C1s spectrum at about 284.6, 286.2, 287.6, and 288.5 eV, belong to the C–C/C–H, C–O, O=C–NH and O=C–O species respectively (Fig. S3B).

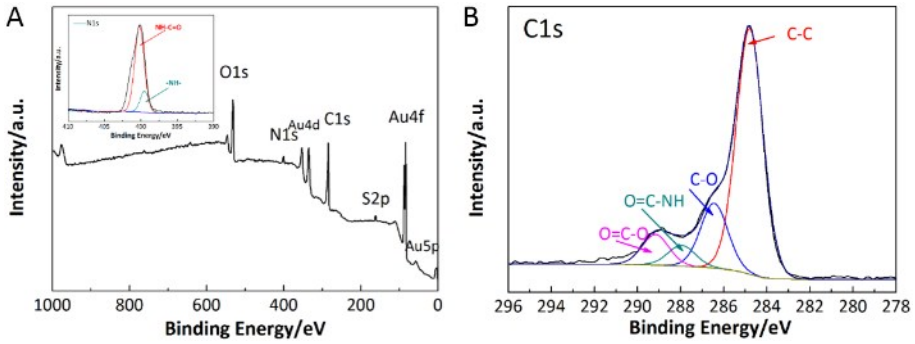

Fig. S3 (A) XPS survey (inset N1s), and (B) C1s spectra of v-SWCNTs(R) prepared on R-SAM/Au.

Comparing with the R-SAM/Au and S-SAM/Au, there are two strong bands around 1590 cm^{-1} (G-band) and 180 cm^{-1} (radial breathing mode, RBM), and a weak band at 1350 cm^{-1} (D-band) of v-SWCNT(S) and v-SWCNT(R). As we know, the presence of RBM is unique to single-walled carbon nanotubes.

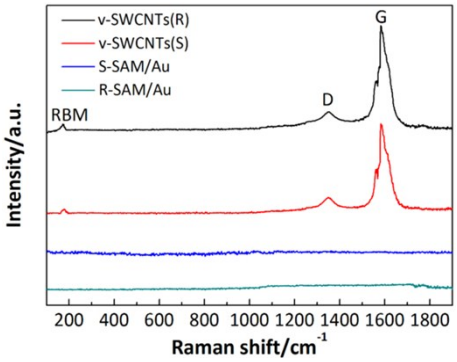

Fig. S4 Raman spectra of the S-SAM/Au, R-SAM/Au, v-SWCNTs(S) and v-SWCNTs(R) respectively.

The BEs in N1s spectra at about 398.9 are attributed to the N–C (Fig. S5A and Fig. S5B), confirming the successful graft of functional molecules on the glass carbon substrates. Meanwhile, the BEs at about 399.4 eV belong to the –NH–, which could be used as anchoring sites for the subsequent immobilization of SWCNTs.

Local domains of v-SWCNTs with aggregated bundles were observed on the glass carbon substrate modified with a SAM of ethylenediamine (Fig. S5C). In contrast, highly vertical and homogenous v-SWCNTs were formed on the substrate modified with a SAM of 1,4-benzendiamine (Fig. S5D), and the bundles were less wide. These features are similar with v-SWCNTs fabricated on gold substrates modified with SAMs of 2-aminoethanethiol and 4-aminothiophenol. It should be noted that v-SWCNTs with a lower density and decreased height were prepared in this condition. Comapring with the easy formation of Au-S bonds between –SH and gold substrates, it was more difficult to graft ethylenediamine and 1,4-benzendiamine molecules on the glass carbon substrates through the amine cation radical formation. As a result, available binding sites for subsequent growth of SWCNTs were reduced on glass carbon substrates.

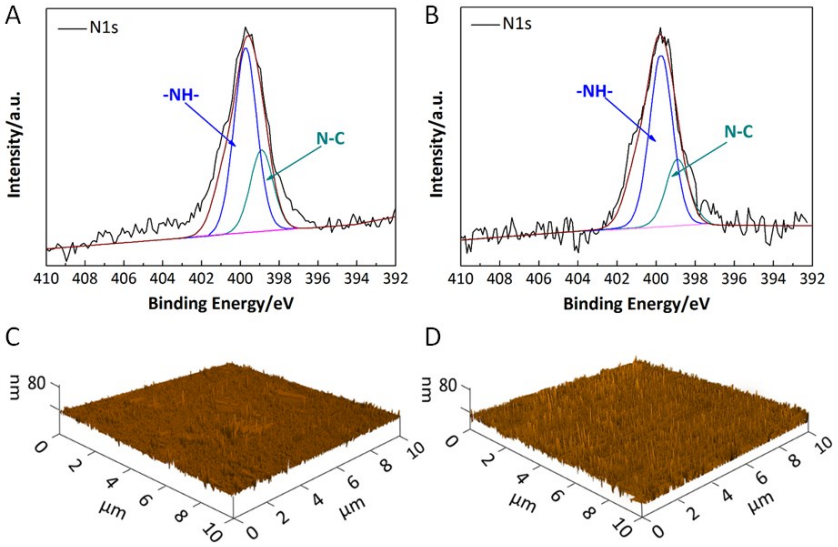

Fig. S5 N1s spectra of (A) ethylenediamine, (B) 1,4-benzendiamine modified glass carbon substrates. AFM images of v-SWCNTs prepared on (C) ethylenediamine and (D) 1,4-benzendiamine modified glass carbon substrates.

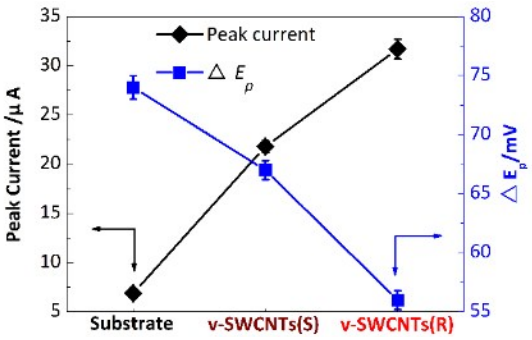

Fig. S6 Corresponding oxidation peak currents (m-RSD of 2.75%) and ΔE_p (m-RSD of 1.43%) of the substrate, v-SWCNTs(S) and v-SWCNTs(R) respectively.

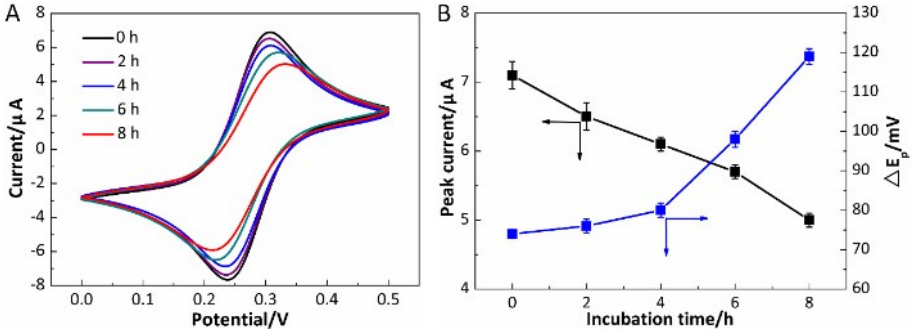

Fig. S7 (A) CV curves of substrates incubating in 4-aminothiophenol solution for various time, in 1 mM $K_3Fe(CN)_6$ containing 0.1 M KCl. (B) Corresponding oxidation peak currents (m-RSD of 3.10%) and ΔE_p (m-RSD of 1.68%) over time.

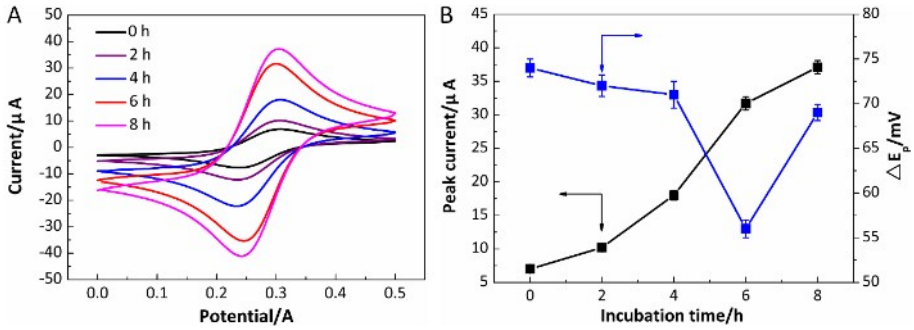

Fig. S8 (A) CV curves of v-SWCNTs(R) fabricated on substrates incubating in the 4-aminothiophenol solution for various time, in 1 mM $K_3Fe(CN)_6$ containing 0.1 M KCl. (B) Corresponding oxidation peak currents (m-RSD of 2.85%) and ΔE_p (m-RSD of 1.35%) over time.

The BEs at 131, 285, 399, 530 and 710 eV are attributed to P2p, C1s, N1s, O1s and Fe2p respectively (Fig. S9A). The BEs in N1s spectrum at about 397.9, 399.4 and 400.2 eV are attributed to the =N–, –NH– and NH–C=O respectively (Fig. S9B). The presence of NH–C=O confirms the effective immobilization of A-probes on MBs, and =N– and –NH– stem from bases in A-probes.

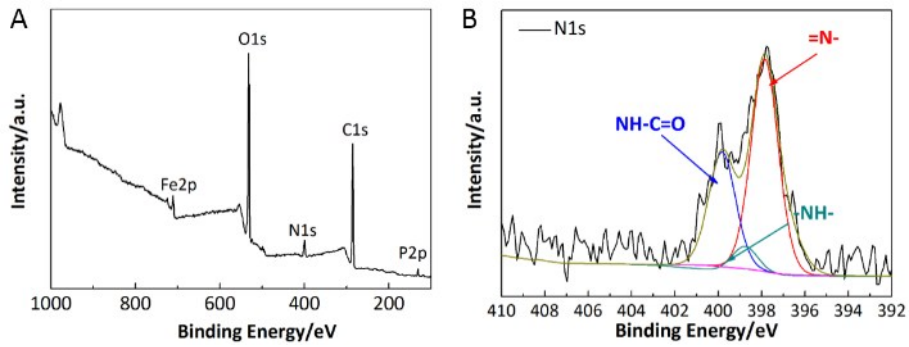

Fig. S9 (A) XPS survey, and (B) N1s spectra of A-probe/MBs.

The BEs at 84, 131, 164, 285, 399 and 530 eV are ascribed to Au4f, P2p, S2p, C1s, N1s and O1s respectively (Fig. S10A). The BEs in N1s spectrum at about 397.9, 399.4 and 400.2 eV belong to the =N–, –NH– and NH–C=O respectively (Fig. S10B). As the R-probes interacted with v-SWCNTs(R) through the π-π interaction, no new chemical bonds is found. The presence of =N– stems from bases in R-probes.

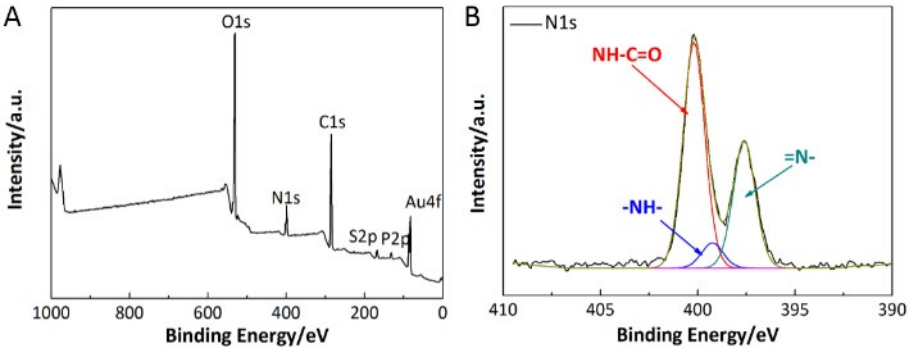

Fig. S10 (A) XPS survey, and (B) N1s spectra of R-probes attached v-SWCNTs(R).

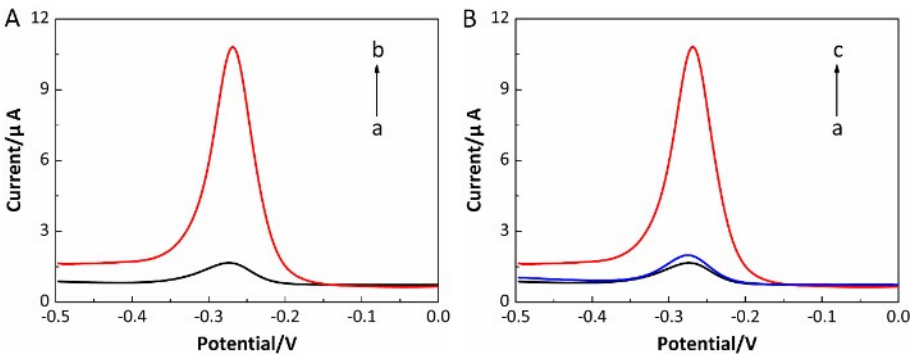

Fig. S11 (A) Feasibility test of the designed sensing scheme, (a) in the absence of Hg^{2+}, (b) in the presence of 0.1 nM Hg^{2+}. (B) Regeneration test of proposed biosensor, (a) in the absence of Hg^{2+}, (b) after the regeneration treatment, (c) in the presence of 0.1 nM Hg^{2+}.

As the hybridization between A-probes and R-probes could be accelerated with a high NaCl concentration, continuously enhanced response signals were acquired with NaCl varying from 0.025 to 0.2 M. However, no obvious change was observed when further increasing NaCl concentration to 0.25 M. As a result, 0.2 M NaCl was introduced in the hybridization process.

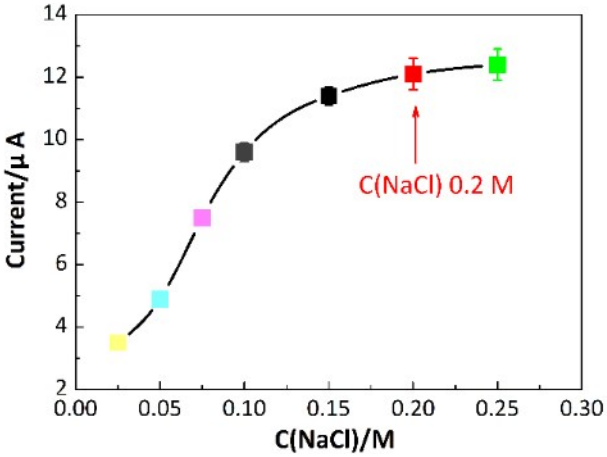

Fig. S12 Optimization of NaCl concentrations for the detection of 1 nM Hg^{2+} (m-RSD of 4.87%).

Table S1 Performance comparisons of different electrochemical Hg^{2+} biosensors.

Sensing materials	Detection limits	Linear ranges	Detection time[a]	Ref.
Gold nanoparticle/DNA	0.5 nM	1 nM-0.1 μM	~1.2 h	12
Gold/DNA	0.1 nM	0.2 nM-100 nM	~1 h	13
Oriented hybrid film/DNA	5 pM	15 pM-0.5 μM	~4 h	35
Gold amalgamation/DNA	20 pM	20 pM-1 μM	~50 min	55
Graphene/DNA	5 nM	8 nM-0.1 μM	~30 min	56
Hemin/DNA	0.5 nM	1 nM-1 μM	~80 min	57
Strepavidin-AgNPs /DNA	24 pM	50 pM-0.1 μM	~2 h	58
Gold/DNA	10 nM	10 nM-0.5 μM	~55 min	59
3DOM PANI-Pt/DNA	87 fM	0.1 pM-1 μM	~80 min	60
v-SWCNTs/DNA	**3 fM**	**10 fM-1 μM**	**~3 h**	**This work**

[a]Assay time is calculated from the Hg^{2+} injection to the readout of the response signal.

Table S2 Assay results of Hg^{2+} in samples of lake water.

Samples	ICP-MS	Found	Recovery/%	RSD/%
1	1.54 nM	1.56 nM	101.3	4.0
2	5.46 nM	5.35 nM	98.0	4.6
3	10.13 nM	10.06 nM	99.3	3.8
4	21.35 nM	21.79 nM	102.9	3.9

Table S3 Assay results of Hg^{2+} in samples of human serum.

Samples	Added	Found	Recovery/%	RSD/%
1	50.00 fM	51.95 fM	103.9	6.1
2	1.00 pM	0.98 pM	98.0	5.9
3	10.00 pM	10.20 pM	102.0	5.6
4	1.00 nM	0.99 nM	99.0	5.5